Available online at www.sciencedirect.com

SciVerse ScienceDirect

Journal of the European Ceramic Society 32 (2012) 2415–2422

www.elsevier.com/locate/jeurceramsoc

Improvement of thermoelectric properties of $Ca_3Co_4O_9$ using soft chemistry synthetic methods

A. Sotelo [a], G. Constantinescu [a], Sh. Rasekh [a], M.A. Torres [b], J.C. Diez [a], M.A. Madre [a,*]

[a] *Instituto de Ciencia de Materiales de Aragón (CSIC-Universidad de Zaragoza), Mª de Luna 3, 50018 Zaragoza, Spain*
[b] *Departamento de Ingeniería de Diseño y Fabricación, Universidad de Zaragoza, Mª de Luna 3, 50018 Zaragoza, Spain*

Received 23 December 2011; received in revised form 6 February 2012; accepted 9 February 2012
Available online 8 March 2012

Abstract

Two solution synthetic methods, sol–gel and a polymeric route, have been studied in order to obtain $Ca_3Co_4O_9$ misfit compounds with improved thermoelectric properties, compared to the classical solid state reaction. A comparison among the final products obtained by these different methods has been performed using DTA, TGA, FTIR, X-ray diffraction, scanning electron microscopy, and thermoelectric characterizations. All the samples obtained by solution synthesis show a very significative reduction on the secondary phases content. As a consequence, an important decrease on the electrical resistivity values is produced, compared to the solid state prepared samples, leading to a relatively important power factor raise.
© 2012 Elsevier Ltd. All rights reserved.

Keywords: Grain growth; Sintering; Microstructure-final; Electrical properties; Thermopower

1. Introduction

Nowadays, thermoelectric (TE) power generation technology is regarded as one of the most promising methods to harvest energy from wasted and/or natural heat sources. In order to reach practical applications, TE materials with high energy conversion efficiency are strongly required for electric power generation. Thermoelectric energy conversion has been shown as an effective technology that can be used to transform thermal to electrical energy. From this point of view, it can help to solve global warming by reducing CO_2 emissions not only due to the efficiency improvement in classical energy transformation systems, but also exploiting natural heat sources. The conversion efficiency of TE materials is quantified by the dimensionless figure of merit, ZT, which is defined as $TS^2/\rho\kappa$ (in which S^2/ρ is also called power factor, PF), where S is the Seebeck coefficient (or thermopower), ρ the electrical resistivity, κ the thermal conductivity, and T is the absolute temperature.[1] From this expression, it is obvious that a performant TE material must posses a high thermopower together with low electrical resistivity and thermal conductivity.

So far, semiconductors and intermetallic materials have been used to manufacture TE modules. On the other hand, they are usually composed of heavy and/or toxic elements which can melt, evaporated or oxidized at high temperatures under air. As a consequence, their use in applications for waste heat recovery at high temperatures presents severe limitations. The solution of these problems started with the discovery of large thermoelectrical properties in a ceramic material, Na_xCoO_2,[2] which was found to posses a high Z value ($8.8 \times 10^{-4}\ K^{-1}$) and large thermopower ($\sim 100\ \mu V\ K^{-1}$) at 300 K. This material is composed of non toxic and cheaper elements than the classical intermetallic ones. Moreover, it can operate at high temperatures, under air, for long time without degradation. As a consequence, this material has opened a new research field in which great efforts have been devoted to explore new CoO families with high thermoelectric performances. Some other layered cobaltites, such as $[Ca_2CoO_3][CoO_2]_{1.62}$ and $[Bi_{0.87}SrO_2]_2[CoO_2]_{1.82}$ were also found to exhibit attractive thermoelectric properties[3–6] which must be increased before they can be used in practical applications.

The crystal structure of these CoO families is composed of two different layers, with an alternate stacking of a common conductive CdI_2-type CoO_2 layer with a two-dimensional triangular

* Corresponding author at: Dept. Ciencia de Materiales, C/Mª de Luna 3, 50018 Zaragoza, Spain. Tel.: +34 976762617; fax: +34 976761957.
E-mail address: amadre@unizar.es (M.A. Madre).

0955-2219/$ – see front matter © 2012 Elsevier Ltd. All rights reserved.
doi:10.1016/j.jeurceramsoc.2012.02.012

lattice and a block layer, composed of insulating rock-salt-type (RS) layers which lead to a very important crystalline and electrical anisotropy. Both sublattices (RS block and CdI_2-type CoO_2 layer) possess common *a*- and *c*-axis lattice parameters and β angles but different *b*-axis length, causing a misfit along the *b*-direction.[7–9] This anisotropy explains the great efforts put on the study of different techniques which can produce polycrystalline materials with their *ab* planes parallelly aligned to the electrical transport direction. Some of these techniques have already shown their potential in increasing the performances of ceramic TE materials, as sinter-forging,[10] template grain growth,[8] spark plasma texturing (SPT),[11] or directional growth from the melt.[12]

On the other hand, the preparation techniques have shown that they can influence drastically the bulk final properties. Moreover, synthetic methods have not yet been enough explored. Commonly, bulk materials are prepared following the classical solid state reaction method, which involves repeated mixing, milling and calcinations. Nevertheless, incomplete reaction, and compositional inhomogeneities are typical trademarks of conventional solid state synthesis. In this context, solution syntheses can offer several advantages, as higher precursor homogeneity and lower particle sizes which lead to higher reactivity. These advantages can produce the improvement of the bulk material properties and/or the reduction of the processing time.

The aim of the present study is developing synthetic methods that yield high-quality $Ca_3Co_4O_9$ powders for their use in practical applications, as TE modules. In this work it will be shown the comparison between three different synthetic methods, conventional solid-state synthesis, sol–gel method and a polymer solution synthesis route,[13,14] and their final bulk properties.

2. Experimental

2.1. Synthesis

The initial $Ca_3Co_4O_9$ powders used in this work were prepared by the classical solid state route and by two solution methods. The preparation methods can be described in detail as follows:

(i) *Solid-state reaction*: $CaCO_3$ (≥99%, Aldrich), and Co_3O_4 (99.5%, Panreac) were ball-milled for 30 min at 300 rpm. The resulting mixture was placed in a furnace and heated slowly to 750 °C, where it was kept for 12 h, followed by furnace cooling. After cooling, the remaining powder was ground and heated again at 800 °C for 12 h, milled and uniaxially pressed at 350 MPa in form of bars (∼3 mm × 3 mm × 14 mm). Finally, the compacts were sintered for 24 h at 900 °C, with final furnace cooling.

(ii) *Sol–gel*: $CaCO_3$ (≥99%, Aldrich) was suspended in a pink solution of $Co(NO_3)_2{\cdot}6H_2O$ (≥99%, Aldrich) in distilled water. Concentrated HNO_3 (analysis grade, Panreac) was added dropwise into the suspension until it turned into a clear solution. Citric acid (99.5%, Panreac) and ethylene glycol (99%, Panreac) were added to this solution in the adequate proportions. Evaporation of the solvent was performed slowly in order to decompose the nitric acid excess, which allows the polymerization reaction between ethylene glycol and citric acid, forming a pink gel. The dried product was then decomposed (slow self combustion) by heating at 350 °C for 1 h. The resulting solid was mechanically ground and calcined at 750 and 800 °C for 12 h, with a manual intermediate grinding. As for the solid state reaction, sintering was performed, following uniaxial pressing at 350 MPa, at 900 °C for 24 h with furnace cooling.

(iii) *Polymer solution synthesis*: $Ca(CH_3CO_2){\cdot}1/2H_2O$ (≥99%, Aldrich) and $Co(CH_3CO_2)_2{\cdot}4H_2O$ (99%, Panreac) were dissolved in distilled H_2O, forming a pink clear solution. Polyethyleneimine (PEI) (50% aqueous, Fluka) was added to the above solution, which turned darker immediately due to the nitrogen–metal bond formation. After partial evaporation (∼80 vol.%) of water in a rotary evaporator, concentrated solution was placed onto a hot plate until a very dark pink paste appeared. Further heating turned this paste to violet colour, followed by a slow combustion with the release of brown fumes (nitrogen oxides). The resulting powder was milled and calcined at 750 and 800 °C for ca. 12 h, with an intermediate milling, uniaxially pressed at 350 MPa, and sintered for 24 h at 900 °C with a final furnace cooling.

2.2. Characterization

In order to characterize the phase evolution, DTA–TGA analyses were performed in a TA Instrument (SDT Q600) system between room temperature and 900 °C. IR spectroscopy has been performed on samples extracted after each processing step in a Bruker IFS 28 Spectrometer, between 1700 and 800 cm^{-1} to determine the extent of calcium carbonate decomposition.

Phase identification has been performed using powder X-ray diffraction (XRD) utilizing a Rigaku D/max-B X-ray powder diffractometer (CuKα radiation) with 2θ ranging between 10 and 70°. Apparent density measurements have been performed on several samples for each synthetic method, as pressed and after sintering, using 4.677 g/cm^3 as theoretical density.[15] Microstructural observations were performed on fractured and polished samples in a JEOL 6000 SEM microscope provided with an Energy Dispersive Spectroscopy (EDS) system, used to determine the elemental composition of each phase. Image analysis has been performed using Digital Micrograph software on several transversal micrographs for each composition in order to estimate the volume fraction of each phase.

Oxygen content was determined in sintered materials by iodometric and cerimetric titrations. In all cases, 100 ml HCl 1 N were kept under Ar flux during at least 1 h in order to evacuate the oxygen from the reaction vessel, avoiding the reactive oxidation. After this process, 50 mg of the powdered sample was added to the acidic solution to be dissolved, together with 80 mg NaI and a drop of starch indicator (iodometry), or 100 mg $FeCl_2$ and a drop of ferroin indicator (cerimetry). In these solutions, Co^{4+} and Co^{3+} are reduced to Co^{2+} while I^- is oxidized to I_3^- (iodometry) and Fe^{2+} to Fe^{3+} (cerimetry). I_3^- is then titrated with 0.02 M $Na_2S_2O_3$ solution, while Fe^{3+} is determined using a 0.015 M $Ce(SO_4)_2$ solution.

Electrical resistivity and thermopower were simultaneously determined for samples obtained by the different synthetic methods, in steady state mode, by the standard dc four-probe

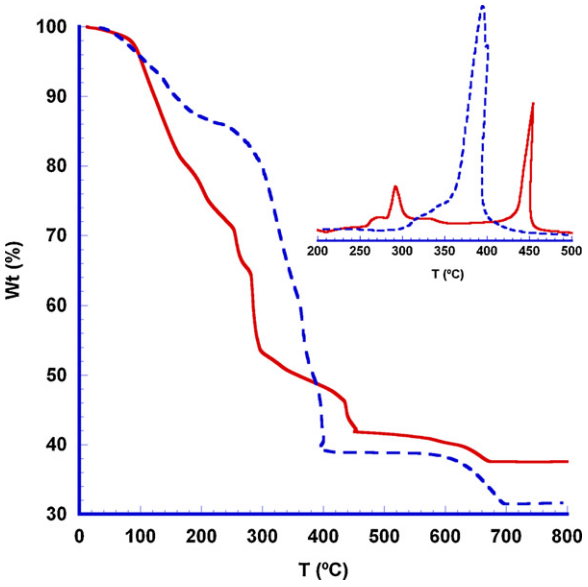

Fig. 1. TGA plots vs. temperature of the dry products obtained by the (—) sol–gel and (- - -) polymer methods. The insert shows the DTA curves in the coordination compounds decomposition temperature range.

technique in a LSR-3 apparatus (Linseis GmBh) between 50 and 800 °C under He atmosphere. With the electrical resistivity and thermopower values, PF has been calculated to determine the TE performances.

3. Results and discussion

3.1. Precursors characterization

DTA–TGA measurements have been performed (under air) on the dry products obtained after evaporation of solvents from the sol–gel and polymer solutions. Fig. 1 represents the weight loss percentage as a function of temperature for all the samples, obtained under similar conditions. As it can be clearly seen in this figure, polymer samples show a broad decomposition step starting at about 300 °C (corresponding to the organic material combustion), while the sol–gel samples decomposed in two steps, the first one starting at around 200 °C, and the second one at about 425 °C. In both cases, this behaviour is confirmed by the DTA graphic shown as an insert in Fig. 1. These different behaviours are most likely related to the different bonding types (metal–nitrogen for the polymer samples and metal–oxygen for the sol–gel ones) and the different decomposition path for the metal–PEI complex, which includes the release of H_2O, CO, CO_2, and NO_x, creating a very reducing atmosphere inside the crucible.[16] This effect clearly explains the higher weight loss for the polymer samples, at 800 °C, compared with the sol–gel ones.

In order to determine the extent of the $CaCO_3$ formation in the as-decomposed coordination compounds, TGA vs. temperature measurements were performed, under air, on all samples. Fig. 2 shows the weight loss percentage with temperature for the sol–gel and polymer samples, together with the initial mixture of $CaCO_3$ and CoO (for the solid state method) used as

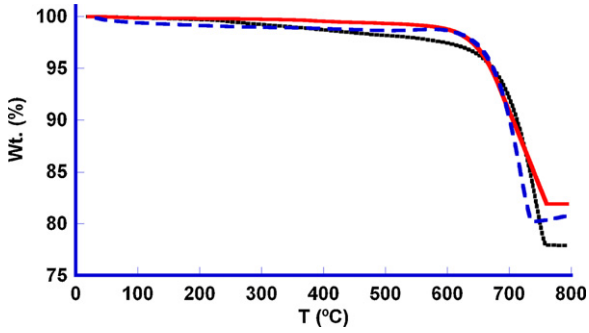

Fig. 2. TGA plots vs. temperature of the as-decomposed products obtained by the (—) sol–gel and (- - -) polymer methods. The initial mixture for the solid state route (■) is included as reference.

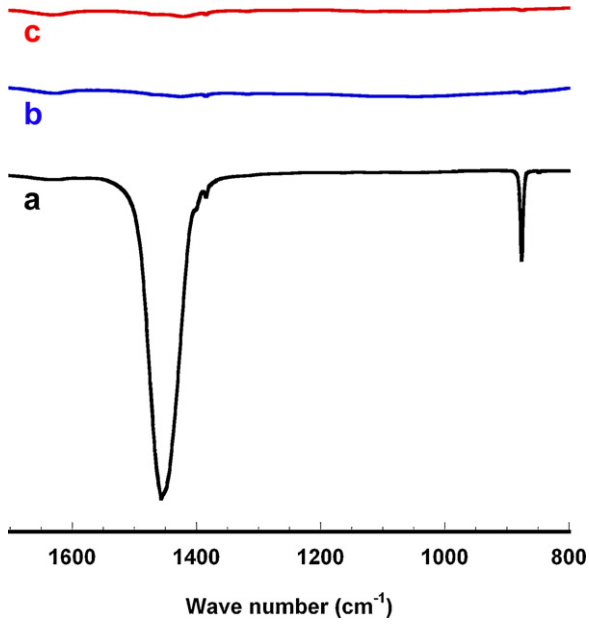

Fig. 3. FTIR curves obtained in different steps of the polymer synthetic procedure: (a) as-decomposed products; (b) after thermal treatment at 750 °C for 12 h; and (c) after calcining at 800 °C for 12 h.

reference. In this figure, it is clear that sol–gel and polymer samples have lower carbonates content than the solid state ones which can be explained by the high temperatures reached in the decomposition process. These high temperature conditions allow, in a certain extent, the reaction between $CaCO_3$ and CoO, producing intermediate reaction products with the subsequent $CaCO_3$ decomposition.

This evolution is confirmed by FTIR spectroscopy which has been performed, between 1700 and 800 cm^{-1}, on all samples before each thermal treatment. All the samples have shown the same behaviour reflected in Fig. 3, where representative samples obtained by the polymer method are presented. Samples after the organic materials decomposition (which correspond to the initial oxides and carbonates mixture for the solid state method) show a very intense band at around 1450 cm^{-1} and a medium one at about 850 cm^{-1}, which are associated to $CaCO_3$ (see Fig. 3a). After the first thermal treatment at 750 °C for 12 h these bands

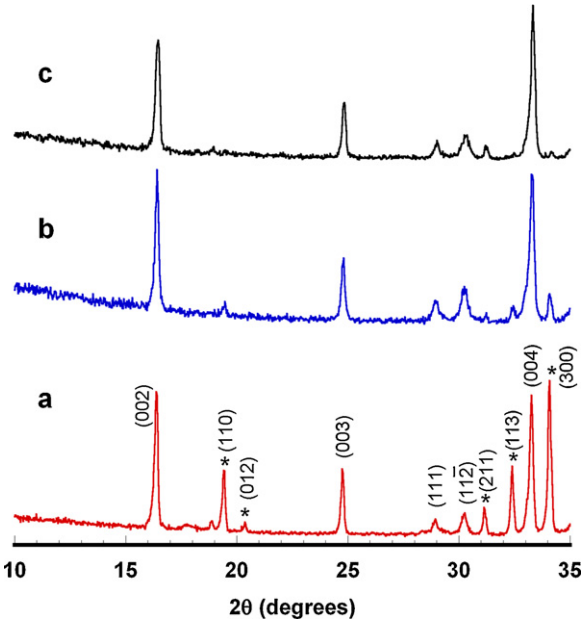

Fig. 4. XRD plots of the $Ca_3Co_4O_9$ sintered specimens obtained for the different synthetic methods. (a) Solid state, (b) sol–gel, and (c) polymer solution. Crystallographic planes are indicated for the $Ca_3Co_4O_9$ phase and $Ca_3Co_2O_6$ one (identified by a *).

disappear, indicating the carbonates decomposition (see Fig. 3b and c).

3.2. Sintered materials characterization

Powder XRD plots for samples obtained for the different synthetic methods are represented (from 10 to 35 degrees for clarity) in Fig. 4. They show similar patterns where the most intense peaks correspond to the crystallographic planes of the $Ca_3Co_4O_9$ cobaltite,[17] indexed in the plot. Other peaks (marked with a * and also indexed in this figure) are associated with the $Ca_3Co_2O_6$ phase[18] which are relatively intense for the solid state synthesized samples (see Fig. 1a) and less important for the ones obtained by solution methods (see Fig. 1b and c). This is a clear indication that, in the synthetic conditions used for the preparation of these samples, the use of solution methods reduces the amount of the undesired $Ca_3Co_2O_6$ phase, evidencing the higher reactivity of the initial powders produced from sol–gel and polymer solution methods. In any case, the $Ca_3Co_4O_9$ phase is the major one, independently of the synthetic route.

Apparent density measurements have been performed on the green bodies obtained after pressing and, subsequently, after sintering. Several samples from each synthetic method have been used in order to obtain accurate density values. The evolution of the bulk density as a function of the synthetic method, as well as the standard error and the percentage of the theoretical density is displayed in Table 1. From these data, it is clear that sol–gel and polymer methods produce higher density green bodies, compared with those produced from the solid state reaction. On the other hand, sintering process increases density inversely to the initial one, leading to very similar ones for the solid state and the sol–gel methods and slightly higher for the polymer solution

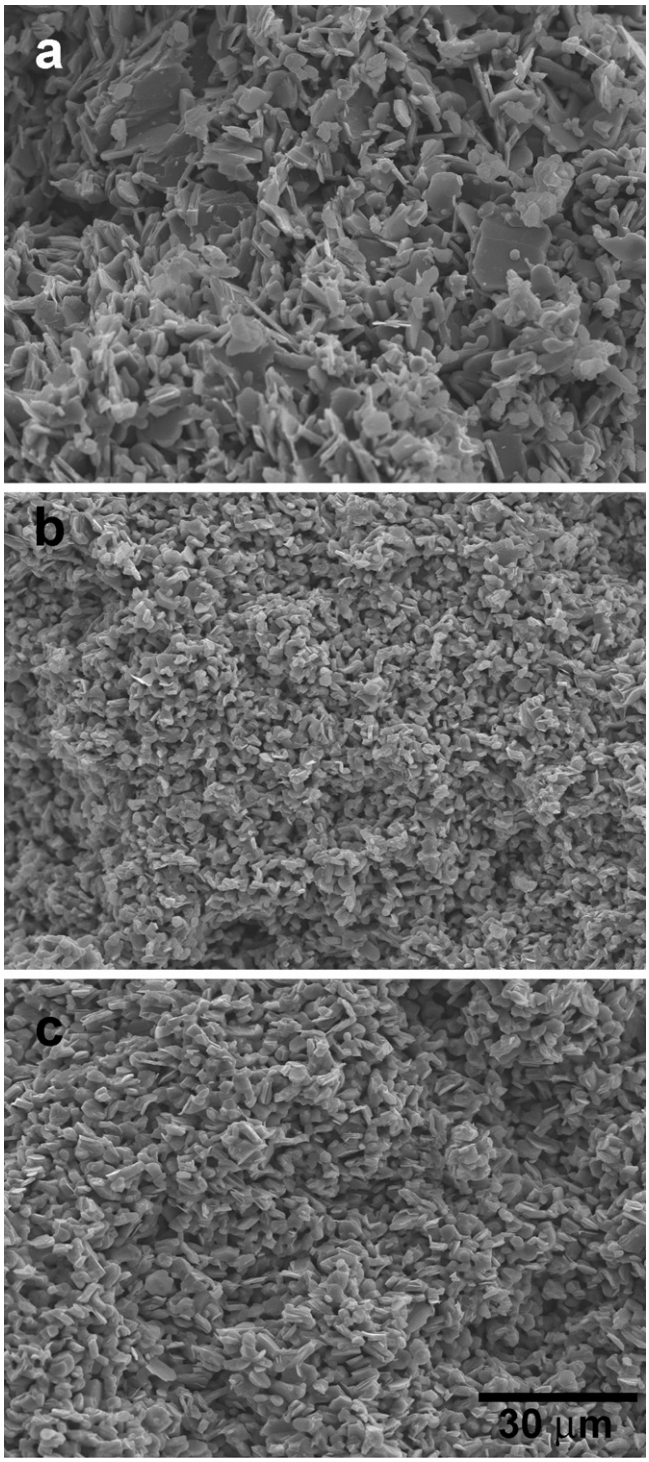

Fig. 5. Scanning electron micrographs obtained on transversal fractured $Ca_3Co_4O_9$ samples prepared by solid-state (a), sol–gel (b), and polymer (c) methods.

samples. Moreover, measured densities for the sintered samples are higher than those reported in the literature for solid state sintered specimens.[15]

SEM micrographs of representative transversal fractures for the different synthetic methods are displayed in Fig. 5. In these images it can be clearly observed that solid state method leads to big plate-like grains together with small ones (see Fig. 5a),

Table 1
Evolution of the mean apparent density of the bulk $Ca_3Co_4O_9$ samples from the green body to the sintered materials for all the samples, together with their standard errors and the % of theoretical density.

	Treatment	Density (g/cm^3)	Standard error	Theoretical density (%)
Solid state	Green body	2.94	0.01	63
	Sintered	3.45	0.01	74
Sol–gel	Green body	3.37	0.01	72
	Sintered	3.47	0.02	74
Polymer	Green body	3.55	0.01	76
	Sintered	3.61	0.02	77

typical feature for the classical synthetic methods. Moreover, solution synthesis leads to smaller grains than the observed in samples obtained by solid state (see Fig. 5b and c) with a very similar grain size all along the bulk material. When comparing the grains produced by the two solution methods, the polymer solution leads to bigger ones than the sol–gel due to the high reactivity observed in the precursor powders obtained by the polymer method, as reported for similarly layered materials.[19,20]

SEM micrographs of longitudinal polished sections of the samples show two main contrasts, as it can be clearly observed in Fig. 6. Major phase in all the studied samples (light grey contrast) has been identified by EDS as the thermoelectric $Ca_3Co_4O_9$ one, except in the zones around the dark grey contrast where some of the grains show the $Ca_3Co_2O_6$ composition while conserving the same observed contrast. Dark grey contrast, appearing as relatively big aggregates, corresponds to CaO which has not been detected in XRD as its (1 1 1) peak appears at around 32.3°,[21] overlapping with the $Ca_3Co_2O_6$ phase (1 1 3) peak. The shape and size of these CaO aggregates change as a function of the synthetic method. For samples prepared by the classical solid state route, they are thick and elongated (see Fig. 6a), reducing the effective conducting section of the ceramic material. When considering samples obtained from the sol–gel method, CaO is found as nearly spherical big aggregates (see Fig. 6b) which also reduce the effective conducting section of these samples, but in lower extent than the observed for the solid state samples. In the case of the polymer solution samples, some CaO is also found but in much lower amount than the obtained in the other two methods.

Other interesting feature observed in these micrographs is related to the porosity which can be observed in Fig. 6 as black spots. In all cases, the pores mean size is reduced from solid state samples to the polymer solution method samples.

The absolute oxygen content was determined on sintered samples using cerimetry and iodometry. For each sample four determinations were performed with each method, showing a reproducibility of around ±0.008 for each method and an agreement of about ±0.01 between the two methods. The obtained mean values are displayed in Table 2. In this table it can be clearly seen that samples obtained by solution methods have approximately the same Co valence (∼3.17) while solid state samples show a lower one (∼3.12). Moreover, the results obtained for the solution samples agree with previous studies that consider the $Ca_3Co_4O_9$ phase as $Ca_9Co_{12}O_{28}$, with the nominal Co valence 3.17.[22]

Table 2
Mean Co valence for all the samples obtained by the two different analytical methods used.

	Method	V_{Co}
Solid state	Cerimetry	3.12
	Iodometry	3.13
Sol–gel	Cerimetry	3.17
	Iodometry	3.18
Polymer	Cerimetry	3.17
	Iodometry	3.16

The temperature (T) dependence of the electrical resistivity (ρ), as a function of the synthetic method, is shown in Fig. 7. As it can be easily seen, two different behaviours are obtained. For the solid state samples, the $\rho(T)$ curve shows semiconducting-like behaviour with very high values in the whole measured temperature range, reaching the lowest value at 800 °C (around $40 \times 10^{-5}\ \Omega\,m$). On the other hand, samples derived from solution methods show very low electrical resistivity values for both synthetic methods, with values around $16 \times 10^{-5}\ \Omega\,m$ in the measured temperature range. Moreover, they reflect a behaviour change at about 400 °C, from semiconducting-like ($d\rho/dT \leq 0$ under 400 °C) to metallic-like ($d\rho/dT \geq 0$ above 400 °C) one. The values measured at 50 °C are, approximately, $16 \times 10^{-5}\ \Omega\,m$ for both kind of samples, much lower than the obtained for the solid state sample (around $70 \times 10^{-5}\ \Omega\,m$) due to the lower amounts of secondary phases produced when using solution methods. Besides, they are also lower than the usually reported resistivities for sintered specimens, about $40 \times 10^{-5}\ \Omega\,m$ at room temperature,[4,23] which is a consequence of the higher density and homogeneity of the samples prepared in this work by solution methods.

Fig. 8 displays the variation of the thermopower as a function of temperature for the three studied methods. All samples exhibit positive values in the whole studied temperature range, confirming a dominating hole conduction mechanism. The obtained values are very similar for all the samples and slightly higher than those reported elsewhere (∼125 $\mu V\,K^{-1}$) at room temperature.[24,25] These values correspond to Co valences around 3.55 when using Koshibae's expression,[26] much higher than those obtained experimentally for all the samples. Moreover, these mean Co valences values agree with previously reported results on this material,[27] indicating that a low spin

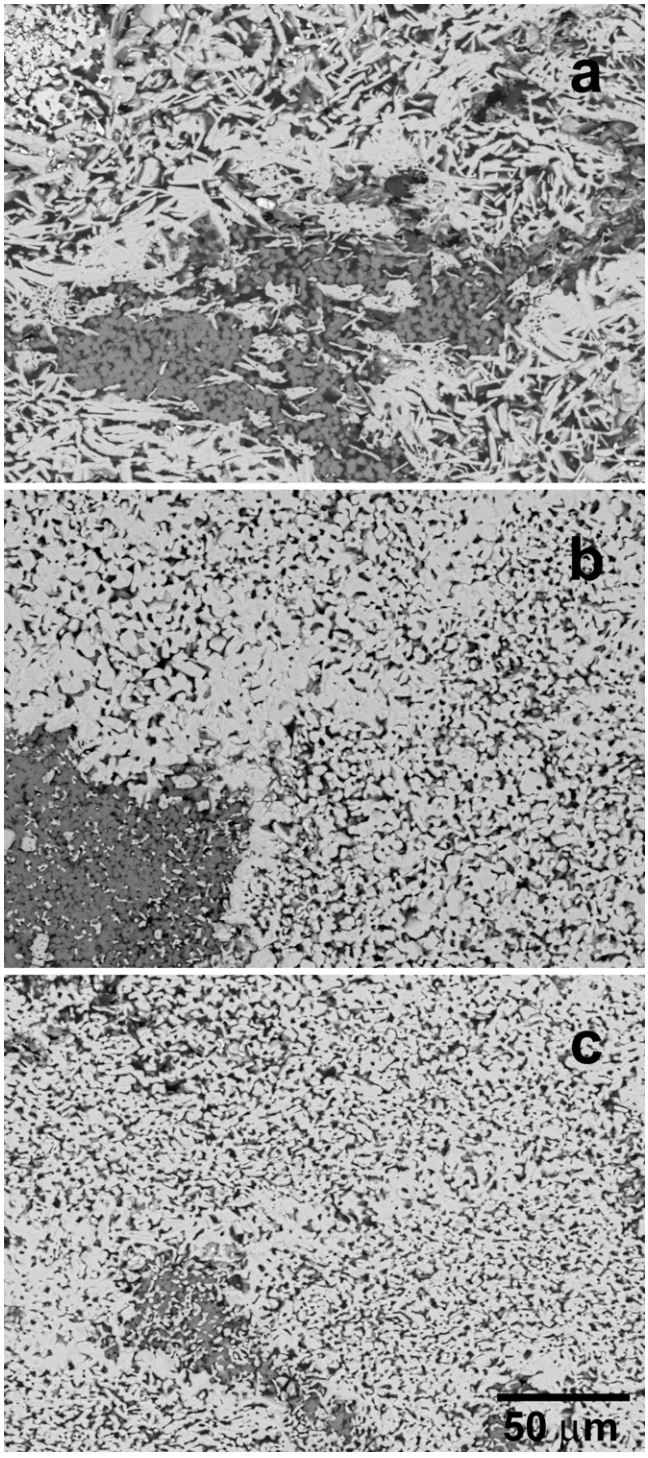

Fig. 6. Scanning electron micrographs from longitudinal polished $Ca_3Co_4O_9$ samples obtained by solid-state (a), sol–gel (b), and polymer (c) reaction methods. Light grey contrast corresponds to the thermoelectric $Ca_3Co_4O_9$ phase, except in the zones around the dark grey contrast (associated to CaO) where the composition changes to $Ca_3Co_2O_6$.

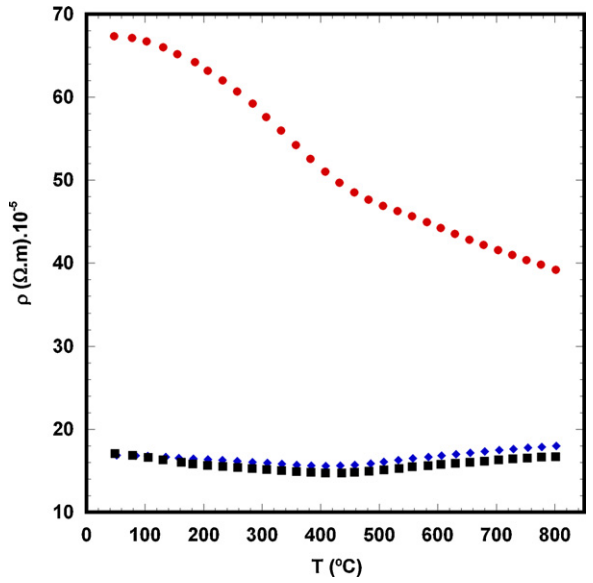

Fig. 7. Temperature dependence of the electrical resistivity for $Ca_3Co_4O_9$, as a function of the synthetic method. (●) Solid state; (♦) sol–gel; and (■) polymer solution.

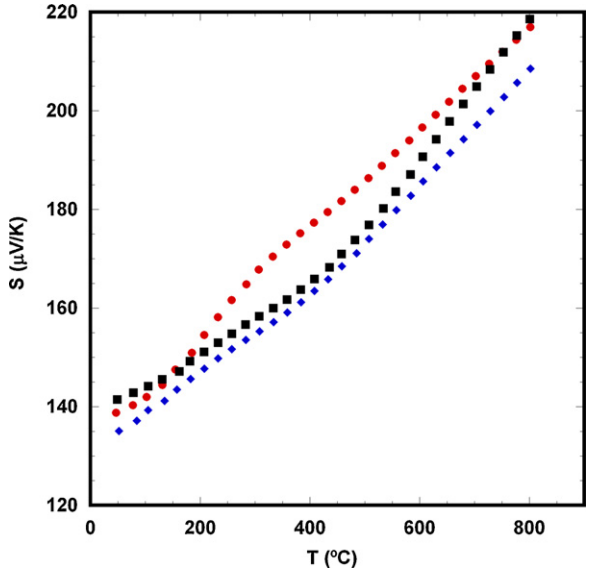

Fig. 8. Temperature dependence of the thermopower for $Ca_3Co_4O_9$, as a function of the synthetic method. (●) Solid state; (♦) sol–gel; and (■) polymer solution.

system model is not adequate for describing the global thermoelectric behaviour of this kind of materials.

From the electrical resistivity and thermopower values, PF variation with temperature has been calculated for all the samples and represented in Fig. 9. From this figure, it is clear that solution methods lead to very similar PF values which are around three times higher than the obtained for solid state prepared samples. When considering PF values at around 700 °C for samples obtained by solution methods ($\sim 20 \times 10^{-5}$ W/K^2 m), they are about two times higher than the highest values reported using the conventional solid state method ($\sim 12 \times 10^{-5}$ W/K^2 m).[22] On the other hand, these values are around one half of the obtained values in textured materials produced by one of the newest texturing methods, the SPT technique ($\sim 40 \times 10^{-5}$ W/K^2 m at 550 °C).[11] This result is an indication of the high quality of powders produced by solution methods,

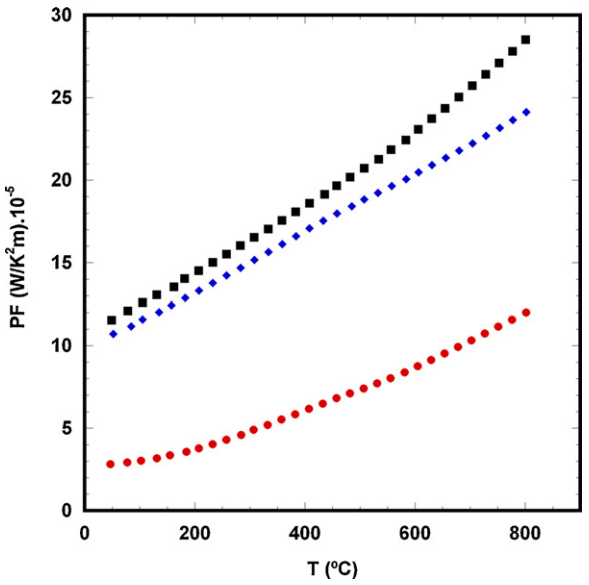

Fig. 9. Temperature dependence of the power factor for $Ca_3Co_4O_9$, as a function of the synthetic method. (●) Solid state; (♦) sol–gel; and (■) polymer solution.

taking into account that the samples presented in this work posses randomly oriented grains.

All the results indicate that solution synthetic routes produce high quality and homogeneous ceramic powders which, when appropriately compacted and sintered, lead to ceramics with low electrical resistivity using very simple and reproducible processes. These reasons make these methods as good candidates for the preparation of bulk ceramics for use in commercial thermoelectric generators or as raw materials to produce materials with highly oriented grains using new texturing techniques, as the SPT method.

4. Conclusions

A comparison of several synthetic routes for obtaining the $Ca_3Co_4O_9$ phase, solid-state, sol–gel and polymer solution, has been made. The typical solid-state method results in a relatively good quality product, but the solution methods evaluated in this study provide much higher yields of the cobaltite phase and better thermoelectrical properties. The main improvement on the electrical properties is due to the very important reduction of secondary phases obtained with the solution methods which lead to PF values about two times higher than the best reported values obtained in samples prepared by the classical solid state method. Furthermore, PF values are closer to the values obtained on textured $Ca_3Co_4O_9$ than the materials produced by other non texturing techniques.

Acknowledgements

This research has been supported by the Spanish Ministry of Science and Innovation-FEDER (Project MAT2008-00429). The authors wish to thank the Gobierno de Aragón (Consolidated Research Groups T87 and T12) for financial support and to C. Estepa, C. Gallego and J.A. Gomez for their technical assistance. Sh. Rasekh acknowledges a JAE-PreDoc 2010 grant from CSIC.

References

1. Rowe DM, editor. *Thermoelectrics handbook: macro to nano*. 1st ed. Boca Raton, FL: CRC Press; 2006. p. 1-3–1-7.
2. Terasaki I, Sasago Y, Uchinokura K. Large thermoelectric power in $NaCo_2O_4$ single crystals. *Phys Rev B* 1997;**56**:12685–7.
3. Funahashi R, Matsubara I, Ikuta H, Takeuchi T, Mizutani U, Sodeoka S. An oxide single crystal with high thermoelectric performance in air. *Jpn J Appl Phys* 2000;**39**:L1127–9.
4. Masset AC, Michel C, Maignan A, Hervieu M, Toulemonde O, Studer F, et al. Misfit-layered cobaltite with an anisotropic giant magnetoresistance: $Ca_3Co_4O_9$. *Phys Rev B* 2000;**62**:166–75.
5. Leligny H, Grebille D, Perez O, Masset AC, Hervieu M, Raveau B. A five-dimensional structural investigation of the misfit layer compound $[Bi_{0.87}SrO_2]_2[CoO_2]_{1.82}$. *Acta Cryst B* 2000;**56**:173–82.
6. Maignan A, Pelloquin D, Hébert S, Klein Y, Hervieu M. Thermoelectric power in misfit cobaltites ceramics: optimization by chemical substitutions. *Bol Soc Esp Ceram V* 2006;**45**:122–5.
7. Maignan A, Hébert S, Hervieu M, Michel C, Pelloquin D, Khomskii D. Magnetoresistance and magnetothermopower properties of Bi/Ca/Co/O and Bi(Pb)/Ca/Co/O misfit layer cobaltites. *J Phys: Condens Matter* 2003;**15**:2711–23.
8. Itahara H, Xia C, Sugiyama J, Tani T. Fabrication of textured thermoelectric layered cobaltites with various rock salt-type layers by using *b*-$Co(OH)_2$ platelets as reactive templates. *J Mater Chem* 2004;**14**:61–6.
9. Guilmeau E, Mikami M, Funahashi R, Chateigner D. Synthesis and thermoelectric properties of $Bi_{2.5}Ca_{2.5}Co_2O_x$ layered cobaltites. *J Mater Res* 2005;**20**:1002–8.
10. Fukutomi H, Konno Y, Okayasu K, Hasegawa M, Nakatsugawa H. Texture development of Ca(3)Co(4)O(9) thermoelectric oxide by high temperature plastic deformation and its contribution to the improvement in electric conductivity. *Mater Sci Eng A* 2009;**527**:61–4.
11. Noudem JG, Kenfaui D, Chateigner D, Gomina M. Toward the enhancement of thermoelectric properties of lamellar $Ca_3Co_4O_9$ by edge-free spark plasma texturing. *Scripta Mater* 2012;**66**:258–60.
12. Sotelo A, Guilmeau E, Madre MA, Marinel S, Diez JC, Prevel M. Fabrication and properties of textured Bi-based cobaltite thermoelectric rods by zone melting. *J Eur Ceram Soc* 2007;**27**:3697–700.
13. de la Fuente GF, Sotelo A, Huang Y, Ruiz MT, Badia A, Angurel LA, et al. Polymer solution processing of (Bi,Pb)–Sr–Ca–Cu–O. *Physica C* 1991;**185**(189):509–10.
14. Madre MA, Rasekh Sh Diez JC, Sotelo A. New solution method to produce high performance thermoelectric ceramics: a case study of Bi–Sr–Co–O. *Matter Lett* 2010;**64**:2566–8.
15. Liou YC, Tsai WC, Lin WY, Lee UR. Synthesis of $Ca_3Co_4O_9$ and $CuAlO_2$ ceramics of the thermoelectric application using a reaction-sintering process. *J Aust Ceram Soc* 2008;**44**:17–22.
16. Sotelo A, de la FuenteF G.F, Lera F, Beltrán D, Sapiña F, Ibáñez R, et al. Novel polymer solution synthesis of the 110K superconducting phase in the bismuth system. *Chem Mater* 1993;**5**:851–6.
17. Brisi C, Rolando P. The calcium oxide-cobalt (II) oxide-oxygen system. *Ann Chim (Rome)* 1968;**58**:676–83.
18. Woermann E, Muan A. Phase equilibria in the system CaO-Cobalt oxide in air. *J Inorg Nucl Chem* 1970;**32**:1455–559.
19. Garnier V, Caillard R, Sotelo A, Desgardin G. Relationship among synthesis, microstructure and properties in sinter-forged Bi-2212 ceramics. *Physica C* 1999;**319**:197–208.
20. Sotelo A, Rasekh Sh, Madre MA, Diez JC. Precursor influence on the electrical properties of textured Bi-2212 superconductors. *J Supercond Nov Magn* 2011;**24**:19–25.
21. Huang Q, Chmaissem O, Capponi JJ, Chaillout C, Marezio M, Tholence JL, Santoro A. Neutron powder diffraction study of the crystal structure of $HgBa_2Ca_4Cu_5O_{12+\delta}$ at room temperature and at 10 K. *Physica C* 1994;**227**:1–9.

22. Li S, Funahashi R, Matsubara I, Ueno K, Yamada H. High temperature thermoelectric properties of oxide $Ca_9Co_{12}O_{28}$. *J Mater Chem* 1999;**9**:1659–60.
23. Kenfaui D, Bonnefont G, Chateigner D, Fantozzi G, Gomina M, Noudem JG. Ca(3)Co(4)O(9) ceramics consolidated by SPS process: optimisation of mechanical and thermoelectric properties. *Mater Res Bull* 2010;**45**:1240–9.
24. Wang Y, Sui Y, Wang X, Su W, Liu X. Enhanced high temperature thermoelectric characteristics of transition metals doped $Ca_3Co_4O_{9+\delta}$ by cold high-pressure fabrication. *J Appl Phys* 2010;**107**:033708.
25. Liu HQ, Zhao XB, Zhu TJ, Song Y, Wang FP. Thermoelectric properties of Gd, Y co-doped Ca(3)Co(4)O(9 + delta). *Curr Appl Phys* 2009;**9**: 409–13.
26. Koshibae W, Tsuitsui K, Maekawa S. Thermopower in cobalt oxides. *Phys Rev B* 2000;**62**:6869–72.
27. Karppinen M, Fjellvåg H, Konno T, Morita Y, Motohashi T, Yamauchi H. Evidence for oxygen vacancies in misfit-layered calcium cobalt oxide, [CoCaO]CoO. *Chem Mater* 2004;**16**:2790–3.